



HAL
open science

Extracting walking trajectories at home from a capacitive proximity sensing floor

M. Sannier, Stefan Janaqi, V. Raducanu, V. Barysheva, H. Ait Haddou, S. Pla, Gérard Dray, Benoît G. Bardy

► **To cite this version:**

M. Sannier, Stefan Janaqi, V. Raducanu, V. Barysheva, H. Ait Haddou, et al.. Extracting walking trajectories at home from a capacitive proximity sensing floor. *IEEE Sensors Journal*, 2022, 22 (4), pp.1-1. 10.1109/JSEN.2021.3139442 . hal-03512496

HAL Id: hal-03512496

<https://imt-mines-ales.hal.science/hal-03512496v1>

Submitted on 31 May 2022

HAL is a multi-disciplinary open access archive for the deposit and dissemination of scientific research documents, whether they are published or not. The documents may come from teaching and research institutions in France or abroad, or from public or private research centers.

L'archive ouverte pluridisciplinaire **HAL**, est destinée au dépôt et à la diffusion de documents scientifiques de niveau recherche, publiés ou non, émanant des établissements d'enseignement et de recherche français ou étrangers, des laboratoires publics ou privés.



Distributed under a Creative Commons Attribution 4.0 International License

Extracting Walking Trajectories at Home From a Capacitive Proximity Sensing Floor

Mélodie Sannier^{1b}, Stefan Janaqi^{1b}, Vinicius Raducanu, Valeriya Barysheva, Hassan Ait Haddou, Simon Pla, Gérard Dray^{1b}, and Benoît G. Bardy^{1b}

Abstract—Walking at home can provide valuable information about locomotor efficiency, anticipation of daily hazards and general well-being. Here, we present a multidisciplinary method to reconstruct locomotor trajectories while walking at home with a capacitive proximity sensing device — the SensFloor — which was installed in a real occupied apartment in the city center of Montpellier in France. Our recognition method is based on the spatio-temporal statistical probability of body location corresponding to sensors' activation. The results led to the localization of the inhabitant in the two-dimensional floor space, and their tracking over a 24-hour period. More precisely, our technique enabled us to distinguish human-related behavior from the location of static objects. It also allowed us to successfully identify locomotor trajectories in a highly confined space, including those from two simultaneously walking individuals in different rooms. It allowed us to obtain valuable information on spatial behavior (trajectory, stationarity) but also on temporal behavior (occupancy time, walking duration). As this technique compensates for the already established low accuracy of capacitive sensors, our method offers innovative possibilities to study locomotor metrics at home using relatively inexpensive sensing technology.

Index Terms—Intelligent floor, locomotor trajectories, modeling, SensFloor, walking at home.



I. INTRODUCTION

IN FRANCE, as well as in several other countries, we usually spend around nine hours per day at home [1], and a

Manuscript received October 9, 2021; revised December 17, 2021; accepted December 19, 2021. Date of publication December 30, 2021; date of current version February 11, 2022. This work was supported in part by the European Regional Development Fund (ERDF) through the HUMAN at home project (HUT), in part by the Occitanie Region, and in part by the Montpellier Méditerranée Métropole. The associate editor coordinating the review of this article and approving it for publication was Prof. Subhas C. Mukhopadhyay. (Corresponding author: Mélodie Sannier.)

This work involved human subjects or animals in its research. Approval of all ethical and experimental procedures and protocols was granted by the Local Ethics Committee under Approval No. IRB-EM 2004B, and performed in line with the Declaration of Helsinki.

Mélodie Sannier, Stefan Janaqi, Simon Pla, Gérard Dray, and Benoît G. Bardy are with the EuroMov Digital Health in Motion (DHM), IMT Mines Alès, University of Montpellier, 34000 Montpellier, France (e-mail: melodie.sannier@umontpellier.fr; stefan.janaqi@mines-ales.fr; simon.pla@umontpellier.fr; gerard.drays@mines-ales.fr; benoit.bardy@umontpellier.fr).

Vinicius Raducanu, Valeriya Barysheva, and Hassan Ait Haddou are with the Laboratoire Innovation Formes Architectures Milieux (LIFAM), National Superior School of Architecture of Montpellier (ENSAM), 34070 Montpellier, France (e-mail: vinicius.raducanu@montpellier.archi.fr; archsorbus@gmail.com; hassan.aithaddou@montpellier.archi.fr).

Digital Object Identifier 10.1109/JSEN.2021.3139442

significant portion of that time involves walking, within one room, or from one room to another. In a highly simplified way, where we live can be represented by a set of closed spaces, cluttered with objects and furniture, offering various affordances such as walking around, sitting on, or standing by. From a locomotor viewpoint, these spatial constraints generate specific trajectories, shaped by attractors (e.g., a chair to reach) and repulsors (e.g., an obstacle to avoid). These trajectories are highly personalized, and depend both on the spatial properties of our place and our locomotor habits, such as walking speed, step length, curvature radius, etc. [2], [3]. Walking is a delicate albeit most natural skill that we progressively master throughout our lives [4], [5]. It involves various perceptuo-motor action units, such as direction control [6], balance control [7], [8], head anticipation [9] or general energy optimization [10]. It reveals who we are, how we make ourselves comfortable in our (new) homes, and allows us to estimate our mood [11], personality [12], and general well-being in our daily lives. The study of ordinary locomotion in our habitat is a difficult enterprise as it requires the use of invisible sensors allowing us to track individuals' movements without influencing their natural behavior. In addition, the reconstruction of the tracked trajectories requires a correct

representation of the environment. Here we present the results of an investigation recently conducted in the city of Montpellier, France, in the form of a smart floor installed in a real apartment. This investigation is part of a project called the HUMAN at home project or HUT [13]. The chosen capacitive smart floor — The SensFloor — was selected as a trade-off between cost and availability of commercialized smart devices (see Section II). The followed approach included (i) the installation of the floor, (ii) the development of the Walk@Home algorithm, allowing the probabilistic estimation of spatio-temporal trajectories, (iii) the statistical analysis of human locomotor behavior and space occupancy.

The article is organized in 6 sections. Section II describes the state of the art in the field of capacitive detection hardware. Section III presents the floor. Methods for parameterization, filtering, interpolation and estimation used in the Walk@Home algorithm are developed in section IV. In section V, the results in both controlled tests and natural walking are presented, and section VI highlights some perspectives.

II. RELATED WORK

Currently, the rise of ambient intelligence is leading to a change in everyday environments towards connected spaces [14]. Amongst these ambient intelligence technologies are systems for tracking and identifying individuals in their natural environment, (e.g., shopping malls [15], health care centers [16], manufactures [17], or at home [18]), in order to anticipate individual needs and provide personalized services. Intelligent floors are often developed in order to recognize when elderly people fall, to prevent serious accidents, and to allow a quick intervention of emergency services and staff. Coupled with home automation devices, they enable synchronized alarm systems and automated heating, blinds and lights, depending on the presence of a human [19]. Smart floors are often distinguished from other ambient intelligence technologies by their undetectable nature. Said to be unobtrusive because they are invisible, these devices are less intrusive [19]. Intelligent floors can be designed using various technologies. Pressure and capacitive proximity sensors are often used, as detailed below.

A. Pressure Sensors

Pressure sensors aim to capture the forces applied by an object on the sensing device. They measure pressure, usually expressed in Pascal (Pa), and convert it into an output signal. This technology is commonly based on strain gauges that are in contact with a pressure sensitive element, commonly a diaphragm. The deformation of the diaphragm sensed by the strain gauges results in an electrical output signal, usually corresponding to a voltage. More precisely, pressure sensors seek to determine the force per unit area exerted on the sensor. The pressure (P) is defined as a function of the force (F) and the surface area (S) by the following relationship [20]:

$$P = \frac{F}{S} \quad (1)$$

The advantage of these pressure sensors is that the measurement results obtained are accurate and consistent, and allow

to discriminate between persons of different weights. Existing intelligent floors with pressure sensors include **GAITRite**, a walking analysis device mainly found in laboratories or medical centers [21], **TechStorm**, used for the diagnosis of sports performance [22] or **LightSpace**, a recreational luminous game responding to step pressure [23].

B. Capacitive Proximity Sensors

Capacitive proximity sensors identify the presence of an object thanks to the detection of its electrical conductivity. In their simplest form, they are constituted of two conductive elements separated by a flexible insulator. The value of the capacitance C depends on the distance between these two conductive elements and thus on the thickness of the insulator according to the following relation:

$$C = \epsilon_r \times \epsilon_0 \times \frac{S}{d} \quad (2)$$

where C is the capacitance in Farad; ϵ_r the relative permittivity of the insulator; ϵ_0 the permittivity of the vacuum; S the surface of the sensor in square meters, and d the thickness of the insulator in meters.

The measurement of the capacitance is thus a measurement of the deformation of the insulator induced by the contact of a charged body. This modifies the initially constant field, between the two conductive elements, and thus changes the thickness of the insulator.

This measurement allows the capacitive proximity sensor to collect information on the conductivity of the elements approaching it. Thus, conductive elements, such as metals or ionic waters, induce an activation of those sensors. The human body, belonging to the family of conductors, also induces an action on these sensors and thus, allows capacitive smart floors to detect its presence. When it penetrates the electric field generated by the two conductive elements, it induces a variation of this electric field, leading to the deformation of the previously mentioned insulator. The sensor will thus send to the output signal an estimate of the variation generated by the body on the sensor. In sum, the more an object is conductive, and the closer it is to the sensor, the more it induces a variation in the electric field, thus the higher its signal will be.

Capacitive proximity sensors have some disadvantages and an important one is that, unlike pressure sensors, they do not provide information about weight. Even very light conductive objects can be detected, which can create noise when data are collected in large areas, and therefore distort measurements. Nevertheless, they have the advantage of being invisible, and, since it is difficult to identify individuals, they ensure confidentiality, a real plus in the area of data protection. Among the already existing capacitive proximity sensor floors on the market are the Elsi Smart Flooring (MarieCare) [24], available on the market since 2010, the FutureShape SensFloor [25], available since 2016, and the imgne® Visible™ smart floor, available since 2019 [26]. For reasons mentioned in Section I, the SensFloor technology was selected in this research.



Fig. 1. Map of the apartment with furniture, sectors arrangement and gaps (green). Each sector is composed of 8 sensors (Insert in red). Gaps are “empty” locations, not equipped with sensors, and are mainly found between rooms or under fixed pieces of furniture. Some sectors were cut during installation.

III. DEVICES AND METHODS

A. The Sensing Floor

The choice of the SensFloor® device was made in 2016, with a limited panel of intelligent floors, as a good compromise between cost and ability to meet the specific requirements of capturing human behavior. The relatively poor spatio-temporal precision we faced led us to develop our own algorithm in order to obtain locomotor trajectories and their associated metrics.

The SensFloor® was installed on almost all of the entire surface of the apartment (72m²), except for a few non-equipable areas, named “gaps.” The floor is three millimeters thick and is composed of a total of 109 sectors. A *sector* is a rectangle (100 cm × 50 cm) designated by the nomenclature XX-YY which represents numbers in hexadecimal format. Each sector consists of eight capacitive proximity *sensors*, enumerated from 1 to 8 in clockwise order. The main components of these sensors are triangular “pixels,” 50 cm × 25 cm in size, that allow conductance detection (Fig. 1). The size of the sensors is large compared to other devices (e.g., SpeedLetiX), and therefore a solid layer of algorithmic computation is required.

Each sensor performs a continuous measurement of the electrical capacitance expressed on a scale from 0 to 255, at a sampling rate of 868 Mhz. The specific zero, calibrated at 127 arbitrary units (AU), allows the expression of negative data that reflect, among other phenomena, the withdrawal of the conductive body. The signals emitted by the sensors, called activations, are encoded on a server, stored in a daily “.csv” file, and transferred post-hoc to the Walk@Home team. Each recorded activation generates the following data (Table. I):

- Timestamp: time in the Unix era.
- X: X-axis position of the SensFloor sectors;
- Y: Y-axis position of the SensFloor sectors;
- 1, . . . , 8: Values of the capacities of the 8 sensors of the sector X-Y related to a tree scale ranging

TABLE I

EXAMPLE OF ONE SIGNAL EMITTED BY A SINGLE ACTIVATION

| Timestamp | X | Y | 1 | 2 | 3 | 4 | 5 | 6 | 7 | 8 |
|-------------|---|----|-----|-----|-----|-----|-----|-----|-----|-----|
| 1.54263E+12 | 7 | 10 | 128 | 129 | 127 | 124 | 126 | 127 | 128 | 127 |

from 0 to 255 AU, with a “zero” specific to the device at 127 AU.

As detailed below, the set of parameters determined for our processing algorithm were built on the basis of a SensFloor calibration file, which included data from specific scenarios.

B. Evaluation Scenarios and Natural Observations

In order to build the reconstruction algorithm, determine activation thresholds, obtain controlled walking samples and identify the presence of noise in the signals, five specific scenarios were first rigorously tested:

(A) Linear trajectories performed at different speeds — normal, slow, stumble, accelerated, fast — simulating various daily walking situations;

(B) Curvilinear trajectory performed at normal speed, simulating for instance walking from one room to another, or avoiding an obstacle;

(C) Simultaneous trajectories of two individuals in the same room, testing for the intersection, avoidance, and separation of the two agents;

(D) Simultaneous trajectories of two individuals in two different rooms;

(E) Quiet stance tested with one individual (E.1), or with two individuals engaged in a conversation (E.2);

Three participants (23 years old ± 1) voluntarily participated in the testing. They were brought to the experimental apartment, filled out the informed consent form, were told about the goal of the test, and performed the five scenarios in turn. They performed seven round-trip trials per scenario, yielding a total of 200 round-trip walking or standing trials. The MATLAB R2020a environment was used to write all the scripts for data cleansing, filtering, and processing, as well as for further analyses.

These scenarios were tested in summer 2019 during a period of non-occupancy of the apartment. In addition, in December 2019, a second step involved the recording of the natural walking behaviors of a single person during 24 hours of occupancy. Results from both evaluations, controlled scenarios and natural walking, will be presented in Section 4. Both situations were conducted in accordance with the 1964 Helsinki declaration and its later amendments, and were approved by the HUT ethical committee. Informed consent was obtained from all participants.

IV. DATA PROCESSING

A. Static Graph

The first step was the reconstruction of the static graph of the apartment. The apartment is organized in 9 areas (Fig. 1): Room 1, Room 2, Room 3, Corridor, Kitchen, Entrance, Living room, Bathroom, Restroom. The 109 × 8 sensors paving the apartment can be organized into a static spatial

graph $G_0 = (V_0, E_0)$ accounting for the geometrical shape and constraints when calculating spatial neighborhood of any point on the floor.

A node of G_0 , $v \in V_0$ is a triplet $v = [x, y, s]$, where x, y is the sector identification and $s = 1, \dots, 8$ is the sensor number.

The node v is the least spatial unity, a “pixel,” and corresponds to a right-angled triangle with sides of 25cm and 50cm. These dimensions indicate the precision limits for further calculations. The number of nodes is $|V_0| = 109 \times 8 = 972$. To each $v = [x, y, s]$ is associated the couple of metric coordinate vectors of the nodes of the sensor s , $v \rightarrow [X(v), Y(v)]$. Most nodes are triangles and $X(v), Y(v)$ have three coordinates. Some sectors are cut, e.g. at the borders of a room. In this case, sectors have a trapezoidal shape and $X(v), Y(v)$ have 4 coordinates.

This identification of nodes then allowed to calculate the coordinates of a representative point into the sensor, e.g. its barycenter. An edge $(u, v) \in E_0$ joins the nodes $u, v \in V_0$. The information about the edge (u, v) is contained in two matrices indexed by the nodes:

- *GAP matrix*: The gap information is important as we have to extract the spatial neighborhood of a node. Entries to this matrix tell whether a node u can be reached with a single “step” ($\approx 80cm$, the upper limit of an average step length) from a node v . More precisely, for $u, v \in V_0$, $GAP(u, v) = Inf$ if there is some physical obstacle between u and v , e.g. a wall. When u and v are in the same room then $GAP(u, v) = 0$.
- *Distance Matrices*: Given two nodes u, v two distances are introduced: (i) $Dmean(u, v)$, the Euclidian distance between the barycenters of the sensors u, v ; and (ii) $Dmin(u, v)$, the Euclidian distance between the nearest points of sensors in u, v .

B. Spatial and Temporal Neighborhoods

1) *Identification of Spatial Neighborhood*: The static graph above is needed to calculate spatial neighborhood. The shape of these neighborhoods must fit the floor structure and consider the gaps. This is one of the advantages of graph representation as it fits the shape irregularities of the apartment. For a given node u of G_0 and a spatial radius ρ , we calculate the spatial neighborhood $N(u, \rho)$. For a distance D ($Dmean$ or $Dmin$), $N(u, \rho)$ contains nodes of $v \in V_0$ such that:

Condition 1: $GAP(u, v) = 0$ and $D(u, v) \leq \rho$. This is the “normal” condition. The neighborhood is “circular” and is not “deformed” by the gaps. The dilatation coefficient of time needed to go from u to v is $R(u, v) = 1$.

Condition 2: $0 < GAP(u, v) < Inf$ and $D(u, v) \leq \rho + GAP(u, v)$. This happens in the case of a missing rectangle or for zones with no sensors. Here, the sector on the other side of the gap is the natural neighbor, and this reshapes the spatial neighborhood. The dilatation coefficient here is given by:

$$\begin{aligned} D(u, v) \leq \rho + GAP(u, v) &= \rho \times \left(1 + \frac{GAP(u, v)}{\rho}\right) \\ &= \rho \times R(u, v) \end{aligned} \quad (3)$$

Thus, any neighbor v of u comes with its dilatation coefficient $R(u, v) = 1 + \frac{GAP(u, v)}{\rho}$. Under the hypothesis of a constant velocity displacement, the dilatation factor $R(u, v)$ will multiply the time radius τ (see below) to obtain the temporal neighborhood. The spatial neighborhood is thus:

$$\begin{aligned} N(u, \rho) \\ = \{v \in V_0 | D(u, v) \leq \rho \times R(u, v), GAP(u, v) < Inf\} \end{aligned} \quad (4)$$

2) *Identification of the Temporal Neighborhood*: Neighborhood identification requires considering the temporal proximity of the node (defined in milliseconds). The static node $u = [x, y, s]$ of G_0 becomes dynamic $u(t) = [x, y, s, t]$ when its activation at time t is considered. When detecting trajectories, dynamic nodes that are “near”- spatially and temporally - are searched for. Given a temporal radius τ , the temporal neighborhood of $u(t)$ is:

$$H(u(t), \tau) = \{v(t') | |t - t'| \leq \tau \times R(u, v)\} \quad (5)$$

The spatio-temporal neighborhood of $u(t)$ is:

$$V(u(t), \rho, \tau) = \{v(t') | GAP(u, v) < Inf, D(u, v) \leq \rho \times R(u, v), |t - t'| \leq \tau \times R(u, v)\} \quad (6)$$

We defined a *trajectory* as a sequence $u_k(t_k), k = 1, \dots, m$ s.t. $u_k(t_k) \in V(u_{k-1}(t_{k-1}), \rho, \tau)$. Obviously, the values of ρ, τ have to be set in advance. Spatial and temporal radii, as well as filtering thresholds (see below) were defined by biomechanical considerations and a trial-and-error process until obtaining the real trajectories of the evaluation scenarios.

C. Filtering

Filtering is an essential component of data processing. As capacitive sensors are sensitive to capacitance, i.e. changes in an electrical property, all recorded activation values (2,119,640) from one raw data file are not valid activations. Three specific filters were here selected and applied in turn.

1) *Activation Filtering*: Let $s_i(t)$ be the signal value of sensor $i, i = 1, \dots, 8$ at instant t . The first filter allowed us to set to 0 all recorded values with $s_i(t) \leq a = 130$, and to retain only those rows of data with at least one $s_i(t) > a = 130$ (Fig. 2a). A large majority of the data was grouped around the value 127, equivalent to the zero of the SensFloor device (section III. A). Preliminary tests allowed us to consider these values around 127 (± 3) as continuous noise related to the device. Applying this filter selected 31.67% of the initial recordings.

2) *Derivative of Activation Filtering*: We observed that when walking on a sector, the value $s_i(t)$ sent by the sector increased, suggesting that the activations of interest are the ones with $\frac{d(s_i(t))}{dt} > \Delta$. The distribution plot of all signal derivatives is given in (Fig. 2b). The comparison of the result of the final trajectories allowed us to confirm the relevance of retaining only the positive derivatives of the signal, representing the specific activations of the capacitive sensors due to walking. We therefore retained only activations with $\frac{d(s_i(t))}{dt} \geq 1$. This filter retained 14.72% of the initial recordings.

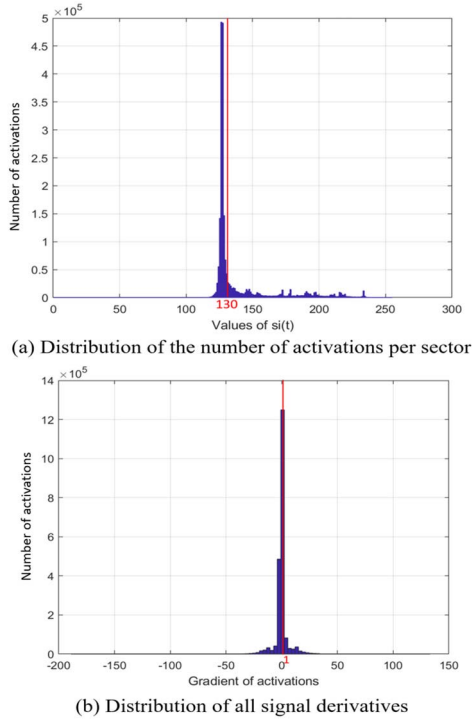


Fig. 2. Bar graph of the distribution of number of activations per sector (a) and signal derivatives (b), used to fix filtering thresholds (in red).

3) *Filtering “Overcrowded” Sectors*: This step was used to neutralize the daily displacement of objects. Global activation was calculated from the number of activations per sector. The results show that, for a continuous daily measurement, 60% of the sectors had no activation, and only a few sectors recorded an abnormally high number of activations (> 1200 activations). These “overloaded” sectors were obviously located under conductive objects, such as the legs of chairs and tables. Hence, only those sectors with a total number of activations lower than 1200 were kept. This filter allowed 95.78% of the initial recordings to pass, so only 4.22% of the initial signals were removed.

These three filters were applied to the data before starting the trajectory identification. Only 25.95% of the rows in the initial data file were found to have at least one valid activation per row after filtering.

D. Walking Trajectory as a Chain of Dynamical Nodes

The dynamic nodes of a given sensor $[x, y, s]$ at time t are defined as $u(t) = [x, y, s, t]$. Our objective was to detect walking trajectories that constitute a “continuous” chain of dynamic nodes, based on the filtered data. A walking path, or trajectory, is defined as a sequence of dynamic nodes:

$$W = u_1(t_1), \dots, u_{k-1}(t_{k-1}), u_k(t_k), \dots, u_w(t_w) \quad (7)$$

such that increasing times is defined by $t_{k-1} < t_k$ for $k = 2, \dots, w$, and continuity is defined by $u_k(t_k) \in V(u_{k-1}(t_{k-1}), \rho, \tau)$, $k = 1, \dots, w$, that is $u_k(t_k)$ is in the spatio-temporal neighborhood of $u_{k-1}(t_{k-1})$ for given radii ρ, τ .

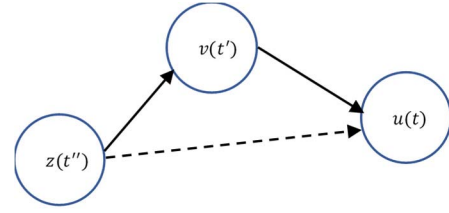


Fig. 3. System representation of the parent-child structure between nodes. The node $z(t'')$ is not allowed to be parent AND grandparent of $u(t)$.

Condition 1 implies a ‘half’ spatio-temporal neighborhood $u_k(t_k) \in V(u_{k-1}(t_{k-1}), \rho, \tau)$ that is:

$$\begin{aligned} GAP(u_{k-1}, u_k) &< Inf \\ D(u_{k-1}, u_k) &\leq \rho \times R(u_{k-1}, u_k) \\ t_k - t_{k-1} &\leq \tau \times R(u_{k-1}, u_k) \end{aligned} \quad (8)$$

The spatial radius ρ and the temporal radius τ here need to be determined. We know that the average human step length is about 64cm (ranging from 50cm to 80cm) and the average step duration, e.g., from right heel strike to left heel strike, is around 500ms [6]. Therefore, we chose the spatial radius $\rho = 60cm$. After several trials and a detailed study of a variety of trajectories, we fixed the temporal radius $\tau = 880ms$. The construction of walking trajectories then followed two steps.

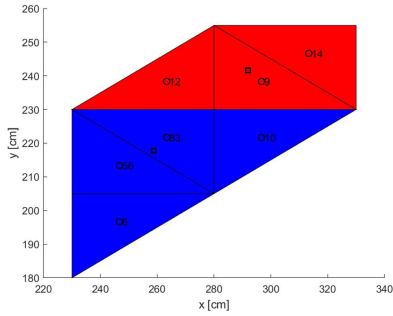
1) *Parent-Child Structure*: The ‘half’ neighborhood suggests organizing the data into a parent-child structure. For each child, that is a dynamical node $u(t)$, we defined its parent(s) $U(t)$ as the set of nodes $v(t')$ such that:

$$\begin{aligned} GAP(u, v) &< Inf, D(u, v) \leq \rho \times R(u, v), \\ 0 &< t - t' \leq \tau \times R(u, v) \end{aligned} \quad (9)$$

Thus, a trajectory arriving at $u(t)$ probably passes through a parent node in $U(t)$ and we noted this relation $U(t) \rightarrow u(t)$. In general, the parent set $U(t)$ contains more than one parent $v(t')$ of $u(t)$ and this parent is merely an eventual predecessor of $u(t)$ in a trajectory. Next, we applied a transitive simplification of parent sets of $u(t)$, and applied a transitive simplification of parent sets. If $z(t'')$ is a parent of $v(t')$ and $u(t)$ and if $v(t')$ is a parent of $u(t)$ then $z(t'')$ is deleted from $U(t)$ (Fig. 3).

2) *Obtaining Trajectories*: The parent-child structure enabled us to organize the dynamic nodes into trajectories. Nodes were ordered by increasing time stamp in a digraph A containing all parent-child arcs, $v(t') \rightarrow u(t)$. This allowed us to calculate the indegree and outdegree for each node $u(t)$. Isolated nodes were eliminated. Each node was assigned at least one path number “NoTraj,” initially set to 0.

The extraction of the chain of dynamic nodes contained in a trajectory was then possible. The resulting dynamic chain was stored in a matrix format. Let us take the example of a dynamic node obtained following this treatment: $u(t) = [3, 5, 1, 23.010]$ and $v(t) = [3, 5, 2, 23.010]$. Here several dynamic nodes have the same timestamp, suggesting that the sensors sent an activation at the same time. Strictly speaking, the activation times of these two sensors differ by less than



Group of sectors at time $t = 0$ and $t = 0.2$

Fig. 4. Representation of two groups of dynamic nodes. Dynamic nodes are in blue at time $t = 0$ and in red at time $t = 0.2$. The circles represent the barycenters of each node. The numbers next to the barycenters are the weighting values $w_j = s_j(t) - 127$. The aggregate point $b(t) = (x(t), y(t))$ is the square. The motion is thus from the blue dynamic node group to the red dynamic node group.

0.001s, allowing them to be discriminated. In order to determine a geometrical curve approximating the real trajectory of the barycenter of one individual, we needed to aggregate these simultaneous dynamic nodes. One robust aggregation method is to take as a representative point the barycenter of the sensors, weighted by their signal level (Fig. 4). All aggregated points were sorted by their unique increasing time stamp. The calculations then yielded a sequence of points such that:

$$XY_{tr} = b(t_k) = (x(t_k), y(t_k)), \quad k = 1, \dots, K \quad (10)$$

Finally, we computed a parametric curve $C(t) = [X(t), Y(t)]$ by fitting with a spline interpolation the points $(t_k, x(t_k))$ into $X(t)$ and $(t_k, y(t_k))$ into $Y(t)$ separately, $k = 1, \dots, K$. The spline interpolation was adopted because it satisfies derivative constraints into the nodes. Note that this choice suggests a smooth locomotion pattern.

V. RESULTS AND DISCUSSION

As mentioned above, we first evaluated our algorithmic approach by testing five controlled scenarios. As the timestamps and the walking conditions are known, this allowed us first to verify the correct functioning of the Walk@Home algorithm. In a second step, we applied our algorithm to a specific data file representing one day of continuous recordings with only one inhabitant in the apartment. We first identified valid trajectories within the apartment, then estimated trajectory-related metrics, and finally performed a statistical analysis of the occupied surface during that day.

A. Controlled Scenarios

1) *Trajectories*: Fig. 5 plots illustrative examples of the trajectories recorded during the controlled manipulation reconstructed by our algorithm in the various scenarios. The reconstructed trajectories in the walking-only (linear (A) and curvilinear (B)) conditions visually correspond to the trajectories imposed before the experiment on the walkers. In the dyadic scenarios, two opposite results were found. The crossing scenario (C) shows the limitation of our algorithm with

TABLE II
PERFORMANCE EVALUATION OF OUR ALGORITHM FROM CONTROLLED SCENARIOS

| | | Comparison of metrics between | | | |
|----|--|-------------------------------|------------------|-------------------|--------|
| | | Controlled scenarios | Algorithm | Error recognition | |
| S1 | Linear trajectories (one person) | Localization of trajectories | Corridor | 0.00% | |
| | Duration (hh:mm:ss) | 00:16:21 | 00:13:35 | 16.94% | |
| | Number of round trips | 105 | 104.5 | 0.48% | |
| S2 | Curvilinear trajectories (one person) | Localization of trajectories | Living & Kitchen | 0.00% | |
| | Duration (hh:mm:ss) | 00:06:21 | 00:04:47 | 24.67% | |
| | Number of round trips | 21 | 20.5 | 2.38% | |
| S3 | Simultaneous trajectories in the same room (two persons) | Localization of trajectories | Living & Kitchen | 0.00% | |
| | Duration (hh:mm:ss) | 00:01:22 | 00:01:55 | 29.76% | |
| | Number of round trips | 20 | 10 | 50.00% | |
| S4 | Simultaneous trajectories in different rooms (two persons) | Localization of trajectories | Room1 & Room3 | 0.00% | |
| | Duration (hh:mm:ss) | 00:02:00 | 00:01:36 | 00:01:40 | 18.37% |
| | Number of round trips | | 6 | 8.5 | |
| S5 | Stationarity stance (one person) | Localization of trajectories | Kitchen | 0.00% | |
| | Duration (hh:mm:ss) | 00:03:00 | 00:02:23 | 20.75% | |
| | Number of round trips | | | | |
| S5 | Stationarity stance (two persons) | Localization of trajectories | Kitchen | 0.00% | |
| | Duration (hh:mm:ss) | 00:01:00 | 00:01:48 | 10.00% | |
| | Number of round trips | | | | |

Note. “S” corresponds to scenario. The temporal value (*duration*) obtained by the algorithm for the duo conditions is the sum of each individual duration. Particularity for pair conditions: (i) The duration obtained with the algorithm is equal to the sum of the duration of each individual of the pair. The recognition error for each trip made in pair is thus a division by 2 of the temporal value (*duration*). (ii) The conditions performed in pairs do not include the number of round trips category (scenario 5).

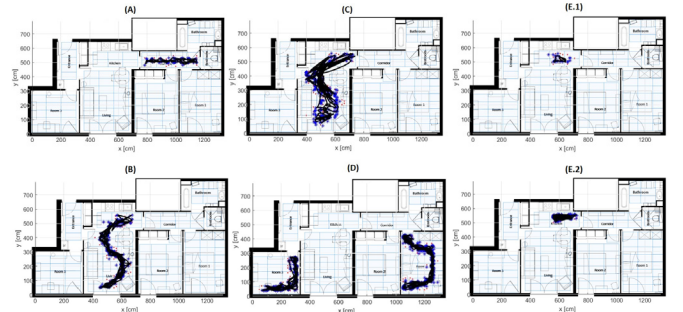


Fig. 5. Typical trajectories obtained from the algorithm in the five tested scenarios. (A) Scenario 1: linear walk in the corridor performed by a single individual, (B) Scenario 2: curvilinear walk in the living room performed by a single individual, (C) Scenario 3: simultaneous walk of two individuals crossing each other in the living room, (D) Scenario 4: simultaneous walk by two individuals in two separate rooms (Room 1 and Room 3), (E) Scenario 5: (1) natural stance (with step trampling and body sway such as, for instance, when doing the dishes) performed by one individual in the kitchen; (2) stationary standing situation performed by two individuals in the kitchen under the same conditions.

frequent confusions between participant 1 and participant 2, when present in the same room. When the two participants are walking in two separate rooms (scenario D), the algorithm picks out the individual trajectories perfectly and simultaneously. This suggests that the limit of our algorithm is not of temporal nature — data belonging to the same time period in different spaces can be correctly associated — but of spatial nature, certainly related to the probability of a wide neighborhood when two individuals are in the same location. The standing scenario performed alone (E.1) is assimilated to a small trajectory made between two sectors, caused by step trampling during quiet stance. As with the dual crossing scenario, the algorithm exhibits confusions between two participants in the dual standing scenario (E.2).

2) *Data Array of the Controlled Scenarios*: Table II compares the spatio-temporal data collected in the control experiment and the data obtained with our algorithm for each walking scenario. Spatial information includes the location of trajectories in the apartment as well as the number of round trips made by each participant. The temporal information corresponds to the time lapse required to make the number of round trips. The error rate between the scenario data and the algorithm data tells us about the recognition efficacy of our algorithm for the following variables.

a) *Localization*: The error rate between performed and reconstructed scenario trajectories was zero for all walking scenarios (1 to 5), alone or in pairs, illustrating the spatial efficacy of the algorithm.

b) *Duration*: The error rate associated with locomotor duration was around 25% for all scenarios. Generally, the algorithm slightly underestimated the temporal aspects of the trajectories.

c) *Number of round trips*: This variable could only be computed for scenarios 1, 2, and 3. For linear and curvilinear trajectories performed alone, the error found was less than 3%. Under the scenario of duo movements in the same room, the error of the algorithm increased to 50%, which is consistent with the results obtained for trajectory identification.

Thus, our algorithm has a good to excellent recognition rate in both spatial and temporal domains, for single individuals walking or standing, or for two individuals when walking in different rooms. When the two individuals are walking (scenario 3) or standing (scenario 5.2) in the same room, errors increase considerably. The most probable reason is the failure to identify spatially neighboring points as belonging to the same individual, and the selected parameters (60cm for step length and 800ms for step duration) will probably need to be adjusted, and/or completed by a second data processing algorithm, in order to account for this multi-person scenario.

B. Natural Walking at Home

The results obtained validate the Walk@Home algorithm and its ability to reconstruct trajectories and extract locomotor parameters (e.g., localization, duration, number of round trips) in controlled scenarios involving one participant, or two participants when not in the same room. In addition, the algorithm can output daily metrics, such as mean distance traveled, mean trajectory duration, mean velocity, or occupancy time per room. Here, we present the first results of a natural scenario corresponding to the real occupation of the apartment by a 22-year-old female inhabitant. One day of occupancy was randomly selected during the 2019-2020 winter season, and the Walk@Home algorithm was used to extract the trajectories and their kinematic properties during that day.

1) *Examples of Trajectory Shapes From Real Data File*: The file “data_8000_2019-12-21_04h20” was randomly selected from all daily files of single occupancy. In order to illustrate the type of data output by the algorithm, Fig. 6 illustrates eight trajectories with different locomotor characteristics. For each of these trajectories, duration, distance travelled, velocity, and localization were automatically provided and are also illustrated. We can observe different trajectory patterns

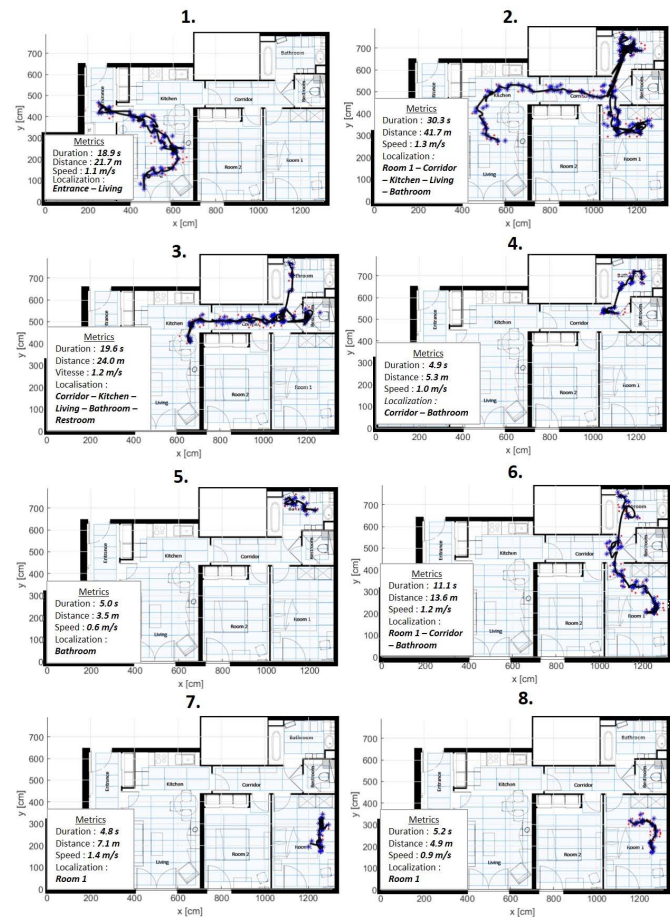


Fig. 6. Illustrations of eight trajectories obtained by algorithmic reconstruction on a real 24-hour file. Each trajectory reports duration (s), walked distance (m), velocity (m/s), and location.

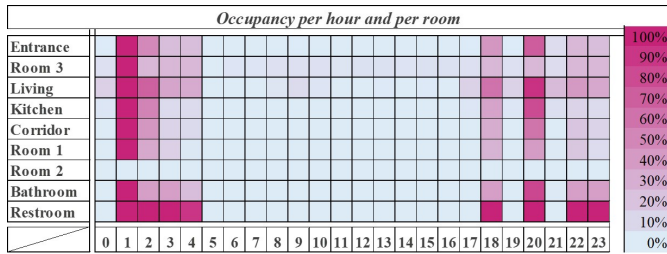
TABLE III
DAILY OCCUPANCY OF THE APARTMENT

| data_8000_2019-12-21_04h20 | | | | |
|----------------------------|--------------------|--|---|---|
| | Occupancy time (s) | Occupancy time in hourly format (HH:MM:SS) | $\frac{T_{\text{Occupancy}}}{T_{\text{Total occupancy}}}$ | $\frac{T_{\text{Occupancy}}}{T_{\text{Total}}}$ |
| Room1 | 1513.71 | 00:25:14 | 21.33% | 1.75% |
| Room2 | 0.00 | 00:00:00 | 0.00% | 0.00% |
| Room3 | 83.82 | 00:01:24 | 1.18% | 0.10% |
| Corridor | 469.05 | 00:07:49 | 6.61% | 0.54% |
| Kitchen | 1248.59 | 00:20:49 | 17.59% | 1.45% |
| Entrance | 199.84 | 00:03:20 | 2.82% | 0.23% |
| Living | 3313.78 | 00:55:14 | 46.69% | 3.84% |
| Bathroom | 132.87 | 00:02:13 | 1.87% | 0.15% |
| Restroom | 135.48 | 00:02:15 | 1.91% | 0.16% |
| Total | 7097.16 | 01:58:17 | 100.00% | 8.21% |

ranging from long trajectories that cross several parts as in examples 1, 2, 3, and 6, to short trajectories, generally localized on a single part, illustrated in examples 4, 5, 7, and 8. In these two cases, in spite of some variability in distance covered and duration, velocity remains constant at around 1m/s.

2) *Global Gait Metrics*: The locomotor information automatically extracted during data processing allowed us to obtain simple daily metrics. For our selected file, “data_8000_2019-12-21_04h20,” 529 trajectories and 595 stationary standing patterns were calculated from 100,490 ground activation contacts. Trajectories were generated with an average velocity of

TABLE IV
OCCUPANCY OF EACH ROOM OVER A 24-HOUR PERIOD



Note. Occupancy, defined by the number of activations per room and per hour, is represented from low (light blue) to high (dark pink).

$\mu_v = 1.4m/s$ ($\sigma_v = 0.6m/s$), for an average distance traveled (per trajectory) of $\mu_l = 14.5m$ ($\sigma_l = 18.9m$) and an average walking time of $\mu_d = 9.4s$ ($\sigma_d = 6.9s$). Each trajectory had an average of 50 activations.

Furthermore, the temporal information extracted showed a dominant occupation of the living room (3.84%) and room1 (1.75%), for a total travel time of 8.21% over a day (Table III).

These metrics, particularly walking velocity (value of $1.4m/s$), are consistent with the literature [27].

3) *Spatial Occupancy*: The matrix shown in Table IV allowed us to obtain a representation of the number of activations per room, broken down into one-hour periods. These data are useful and allow us to (i) observe the occupancy dynamics, (ii) understand the habits of the inhabitants, e.g., the links between occupancy and daily needs (restroom, kitchen, bathroom), and (iii) optimize in the future living spaces according to locomotor habits, personal needs and comfort. We previously tested and validated the calibration file and ensured the consistency of the occupancy data output by the algorithm. We defined here the occupancy of one room by its number of activations per time slot. For instance, the bathroom had its maximum occupancy from 1am to 2am with 512 activations recorded, followed by another intense occupation period from 8pm to 9pm (422 activations). Following this approach, we can easily observe (i) no activation in room 2 witnessing single occupancy, (ii) an intense activity in all other rooms between 1am and 2am, (iii) almost no activity from 5am to 5pm, and (iv) an increase in occupancy starting at 6pm. All together, these results reveal a rather nocturnal way of life, which is compatible with the period, December 21, 2019 being within the holiday season for students in France.

VI. CONCLUSION

The physical limitations of capacitive smart floors require to develop processing algorithms which compensate for the lack of accuracy. Facing one of these systems, the Sens-Floor, our objective was to reconstruct locomotor trajectories produced in a real apartment and to automatically identify the metrics associated with each natural occupancy file. Our method was based on (i) the reconstruction of the static graph, (ii) the identification of the spatial and temporal neighborhoods and the recognition of the temporal sequence of activations, (iii) the cleaning of the data and (iv) the reconstruction of the chain of dynamic nodes allowing to visualize all trajectories.

The implementation of a rigorous protocol allowed us to estimate the processing efficiency of our algorithm for different scenarios in which locomotor trajectories were produced alone or in pairs. We were able to validate the correct functioning of our algorithm for trajectories performed alone, or in pairs, in separate rooms, thus validating the recognition of multiple-activities within the same home. Applied to files from the continuous recording of the occupants' movement data, we were able to explore (i) the various shapes of natural trajectories, (ii) the main walking metrics, and (iii) the evolution of occupancy over a 24-hour period. The main limit of our algorithm remains the spatio-temporal proximity of multiple individuals walking in the same room, which is currently being addressed. The extraction of natural walking patterns over a prolonged period of time (e.g. one year) is also currently being considered. It should help us to better characterize human locomotion at home, space appropriation and the formation of behavioral habits as time goes by allowing us to optimize the human habitat.

REFERENCES

- [1] BVA Survey. (Nov. 2015). *Les Français et Leurs Habitudes au Sein de la Maison*. [Online]. Available: <https://www.bva-group.com/sondages/>
- [2] A.-H. Olivier, A. Marin, A. Créteil, and J. Pettré, "Minimal predicted distance: A common metric for collision avoidance during pairwise interactions between walkers," *Gait Posture*, vol. 36, no. 3, pp. 399–404, Jul. 2012.
- [3] H. Hicheur, S. Vieilledent, M. J. E. Richardson, T. Flash, and A. Berthoz, "Velocity and curvature in human locomotion along complex curved paths: A comparison with hand movements," *Exp. Brain Res.*, vol. 162, no. 2, pp. 145–154, Dec. 2004.
- [4] V. T. Inman, H. J. Ralston, and F. Todd, "Human walking," in *Ergonomics*, vol. 24, no. 12. Baltimore, MD, USA: Williams & Wilkins, 1981, pp. 969–976.
- [5] J. L. Emken, R. Benitez, A. Sideris, J. E. Bobrow, and D. J. Reinkensmeyer, "Motor adaptation as a greedy optimization of error and effort," *J. Neurophysiol.*, vol. 97, no. 6, pp. 3997–4006, 2007.
- [6] D. A. Winter, A. E. Patla, J. S. Frank, and S. E. Walt, "Biomechanical walking pattern changes in the fit and healthy elderly," *Phys. Therapy*, vol. 70, no. 3, pp. 340–347, 1990.
- [7] B. G. Bardy, W. H. Warren, and B. A. Kay, "Motion parallax is used to control postural sway during walking," *Exp. Brain Res.*, vol. 111, no. 2, pp. 271–282, Sep. 1996.
- [8] J. Perry and J. R. Davids, "Gait analysis: Normal and pathological function," *J. Pediatric Orthopaedics*, vol. 12, no. 6, p. 815, 1992.
- [9] B. R. Fajen and W. H. Warren, "Behavioral dynamics of steering, obstacle avoidance, and route selection," *J. Exp. Psychol. Hum. Perception Perform.*, vol. 29, no. 2, p. 343, 2003.
- [10] J. M. Donelan, R. Kram, and A. D. Kuo, "Mechanical and metabolic determinants of the preferred step width in human walking," *Proc. Roy. Soc. B*, vol. 268, pp. 1985–1992, Oct. 2001.
- [11] J. Michalak, N. F. Troje, J. Fischer, P. Vollmar, T. Heidenreich, and D. Schulte, "Embodiment of sadness and depression—Gait patterns associated with dysphoric mood," *Psychosomatic Med.*, vol. 71, no. 5, pp. 580–587, 2009.
- [12] N. F. Troje, "Decomposing biological motion: A framework for analysis and synthesis of human gait patterns," *J. Vis.*, vol. 2, no. 5, p. 2, Sep. 2002.
- [13] *Human at Home Project*. Accessed: 2020. [Online]. Available: <https://www.hut-occitanie.eu/>
- [14] D. J. Cook, J. C. Augusto, and V. R. Jakkula, "Ambient intelligence: Technologies, applications, and opportunities," *Pervas. Mobile Comput.*, vol. 5, no. 4, pp. 277–298, Aug. 2009.
- [15] M. A. Sarwar, Y. A. Daraghmi, K. W. Liu, H. C. Chi, T. U. Ík, and Y. Li, "Smart shopping carts based on mobile computing and deep learning cloud services," in *Proc. IEEE WCNC*, May 2020, pp. 1–6.
- [16] P. Y. Durand *et al.*, "DIATELIC: A new «Intelligent» telemedicine system to avoid hydration disorders in CAPD patients," in *Peritoneal Dialysis International*, vol. 20. Milton, ON, Canada: Multimed, 2000.

- [17] D. Mishra, N. R. Zema, and E. Natalizio, "A high-end IoT devices framework to foster beyond-connectivity capabilities in 5G/B5G architecture," *IEEE Commun. Mag.*, vol. 59, no. 1, pp. 55–61, Jan. 2021, doi: [10.1109/MCOM.001.2000504](https://doi.org/10.1109/MCOM.001.2000504).
- [18] C. D. Kidd *et al.*, "The aware home: A living laboratory for ubiquitous computing research," in *Proc. IWCB*. Berlin, Germany: Springer, 1999, pp. 191–198.
- [19] M. Andries, "Object and human tracking, and robot control through a load sensing floor," Ph.D. dissertation, Univ. Lorraine, Nancy, France, 2015.
- [20] B. Pascal, *Traité de L'équilibre des Liqueurs et de la Pesanteur de la Masse de L'air*, vol. 1648. Paris, France: G. Desprez, 1956, ch. 1.
- [21] B. Bilney, M. Morris, and K. Webster, "Concurrent related validity of the GAITRite walkway system for quantification of the spatial and temporal parameters of gait," *Gait Posture*, vol. 17, no. 1, pp. 68–74, Feb. 2003.
- [22] *TechStorm Foot Scan*. Accessed: 2021. [Online]. Available: <http://techstorm.koreasme.com/pro/pro09.html>
- [23] The Active Gaming Company. *Lightspace Floor*. Accessed: 2020. [Online]. Available: <http://www.the-agc.com/products/physical-therapy/lightspace-floor/>
- [24] *MarieCare*. Accessed: 2020. [Online]. Available: <https://maricare.com/en>
- [25] FutureShape. *SensFloor*. Accessed: 2019. [Online]. Available: <https://future-shape.com/>
- [26] *The Imgne® Visible™ Smart Floor*. Accessed: 2020. [Online]. Available: <http://imgne.com/>
- [27] B. L. Day and S. R. Lord, "Balance, gait, and falls," in *Handbook of Clinical Neurology*, vol. 159. Amsterdam, The Netherlands: Elsevier, Nov. 2018, ch. 13, pp. 205–228.



Mélodie Sannier was born in Martinique. She received the B.S. degree in science, technology, and health from the University of the French West Indies in 2017 and the M.S. degree in engineering for health from the University of Montpellier, France, in 2019, where she is currently pursuing the Ph.D. degree in human movement sciences, also pursuing her research on the control of locomotion with the EuroMov Digital Health in Motion (EuroMov DHM) Research Unit. From 2018 to 2019, she worked as a Trainee in the regional HUMAN at home project (HUT), where she was involved in the calibration and analysis of the SensFloor device.



Stefan Janaqi is a Senior Lecturer at the EuroMov Digital Health in Motion (DHM) Research Unit, IMT Mines Alès. His research concerns mathematical modeling, particularly optimization methods, applied to machine learning and data science. He is mainly specialized in dimension reduction approaches, with supervised and unsupervised methods. He has several recent contributions to clinical as well as hard core industrial domains.



Vinicius Raducanu graduated from the Ion Mincu University of Architecture and Urbanism, Bucharest, Romania, in 1996, and the National Superior School of Architecture of Montpellier (ENSAM), France, in 2002, and received the Ph.D. degree in civil engineering from the University of Montpellier in 2001. During his Ph.D. degree, he developed innovative tensegrity structures. As an Associate Professor at ENSAM, he pursued his research in-between architecture, parametric design, complex movements,

and structural morphology at the Laboratoire Innovation Formes Architectures Milieux (LIFAM). He now teaches a think high-tech and act low-tech outlook in architecture. As an Associate of Atelier Méditerranéen, he promotes a collective and interdisciplinary practice in the ecological shift in architecture and urban design.



Valeriya Barysheva received the master's degree in architecture from the National Superior School of Architecture of Montpellier (ENSAM), France. During her research internship, she proposed a project for the studio "Art and Architecture" entitled "Salins, Villeneuve les Maguelone," and contributed to the Walk@Home research activities at the interface between architecture and movement sciences.



Hassan Ait Haddou received the Habilitation degree in 2018. He is an Associate Professor of Informatics at the National Superior School of Architecture of Montpellier (ENSAM) and the Director of the Laboratoire Innovation Formes Architectures Milieux (LIFAM). In his research, he combines modeling and simulation of complex phenomena, decision-making tools, and environmental performance of architectural and urban forms. The main purpose of his work is to develop models, decision support tools (DST), and decision support systems (DSS) for architects and urban planners.



Simon Pla received the M.Sc. degree in physics and the M.Sc. degree in microelectronics from Paul Sabatier University, Toulouse, in 1994 and 1995, respectively. From 1998 to 2009, he worked for the Centre de Recherches du Service de Santé des Armées, La Tronche, Isère, France, as an Electronics Engineer, for the Laboratoire Sols, Solides, Structures, Risques (3SR), Grenoble University, as an Instrumentation Engineer from 2009 to 2013, and for the Centre National de la Recherche Scientifique, Grenoble, as an Electronics Engineer from 2013 to 2014. Since 2014, he has been with the EuroMov Digital Health in Motion (DHM), University of Montpellier, as an Instrumentation Engineer.



Gérard Dray is a Full Professor at the EuroMov Digital Health in Motion (DHM) Research Unit, IMT Mines Alès. In his research, he develops information processing methods to computerize multimodal cumulative knowledge in order to facilitate human action, making it more reliable and more efficient. These information processing procedures are mainly based on artificial intelligence and machine learning methods. Within the framework of EuroMov DHM, a recent partnership between the University of Montpellier and IMT Mines Alès, he is in charge of the "factory" transverse axis, which aims to improve the reproducibility of clinical results, accelerate translational research, and technology transfer by producing standardized and documented approaches.



Benoît G. Bardy received the Ph.D. and Habilitation degrees in movement sciences from Aix-Marseille University, France, in 1991 and 1998, respectively. In 1994, he was awarded a NATO Research Fellowship to develop his research on locomotion in virtual reality at Brown University, RI, USA. After being selected as a new Professor at the University of Paris (Paris-Sud) in 1999, he entered the prestigious Institut Universitaire de France as a Junior Member from 2001 to 2006. In 2005, he returned to the South of France and created EuroMov, a European center for research, technology, and innovation at the crossover between movement, health, and digital sciences (now EuroMov Digital Health in Motion (DHM), www.euromov.eu). In 2012, he was re-inducted into the Institut Universitaire de France as a Senior Member. His research focuses on perception and action, in real and virtual environments, deploying technology-oriented, rehabilitation, industrial, or artistic solutions. He has coordinated several European, national, and regional initiatives, in both research and research and development projects, and he is a Regular Expert for the European Commission and the private sector. He leads the Walk@Home activities in the HUMAN at home project (HUT).